Journal of Molecular Liquids 392 (2023) 123441

Contents lists available at ScienceDirect

Journal of Molecular Liquids

journal homepage: www.elsevier.com/locate/molliq

Probing the structural organization of a low temperature transition mixture for CO_2 capture through spectroscopic and theoretical studies

Tanja Traini [a], Duccio Tatini [a], Elisa Rossi [b], Gianluca Ciancaleoni [b,*], Pierandrea Lo Nostro [a,*]

[a] Department of Chemistry "Ugo Schiff" and CSGI, University of Florence, 50019 Sesto Fiorentino, Italy
[b] Department of Chemistry and Industrial Chemistry, University of Pisa, 56124 Pisa, Italy

ARTICLE INFO

Keywords:
Low temperature transition mixture
LTTM
Carbon capture
Ethylene glycol
Boric acid

ABSTRACT

We investigated a low temperature transition mixture (LTTM) suitable for carbon capture through infrared spectroscopy, differential scanning calorimetry, absorption of CO_2 and computational studies. The system, made up of a homogeneous mixture of ethylene glycol, potassium hydroxide and boric acid (3:1:1), is sensitive to temperature changes that affect the viscosity of the solvent and its capacity to exchange CO_2 at the interface.

The relationship between the LTTM's molecular structure and its ability to capture the gas were investigated in order to optimize the properties of the absorbing material for developing viable and reusable carbon capture systems.

The results suggest that a large number of free OH groups is available to ensure an effective CO_2 capture through the formation of the organic carbonate, leading to an average absorption of 22 ± 1 g_{CO_2}/kg_{solv} at room temperature. Boric acid acts as a catalyst for the carbonate decomposition and ensures the release of CO_2 at 60 °C.

ATR-FTIR measurements proved that the solvent is mostly regenerated after desorption and can thus continue to absorb further CO_2 over a large number of cycles, making the system reusable.

1. Introduction

Global warming is currently recognized as the biggest and most crucial issue humanity has to face. To meet the Paris Agreement goal to keep the temperature increase below 1.5 °C [1], there is the need to reduce greenhouse gases [2,3] emissions, in particular CO_2, by switching to low-carbon energy sources [4]. But while fossil fuels still continue to be a substantial part of the energy portfolio, CO_2 Capture and Storage (CCS) is a promising candidate to address the problem, even though further implementation work is still needed [5,6]. Currently the traditional method used for carrying out carbon capture is based on the absorption of CO_2 by alkanolamine [7], the benchmark being a 20–30 % aqueous monoethanolamine (MEA) solution. The latter provides a reasonable capture at moderate costs [8], however it has its drawbacks, such as high desorption costs, sorbent evaporation and degradation, or corrosion [9,10].

To replace amine-based absorption, ionic liquids (ILs) have been widely studied as potential candidates for CCS, and recently Deep Eutectic Solvents (DESs) emerged as a new class of IL analogues [11–13]. DESs form via self-association, thanks to the instauration of intermolecular interactions like van der Waals interactions, electrostatic interactions and hydrogen bonding between a hydrogen bond donor (HBD) with a hydrogen bond acceptor (HBA) [18]. For this reason DESs are easier to prepare than ILs, while they also avoid other drawbacks linked to the high viscosity, toxicity and degradability of ILs [14–17].

Because of the dynamic nature of the aggregates, DESs exhibit peculiar physico-chemical properties, such as the eutectic point depression [13], their glass forming ability [18,19] and high viscosity [20]. Moreover, the plentiful availability of different HBDs and HBAs make these properties highly tuneable, which is an essential feature to develop task-specific systems for various applications [21,22].

Because of the strong intermolecular forces, DESs typically show viscosities that are higher than those of other organic solvents. This can lead to complications during their use in CO_2 capture, since high viscosities hamper mass and heat transfer rates and the mobility of dissolved species through the solvent and lead to prohibitive costs of pumping and the need of oversized equipment for CCS. DESs with remarkable low viscosities can be obtained by adding water, which can however compete with CO_2 for the absorption sites [23] and decrease the capturing ability [24]. To avoid this, a good strategy is the inclusion

* Corresponding authors.
E-mail addresses: gianluca.ciancaleoni@unipi.it (G. Ciancaleoni), pierandrea.lonostro@unifi.it (P. Lo Nostro).

https://doi.org/10.1016/j.molliq.2023.123441
Received 16 March 2023; Received in revised form 22 October 2023; Accepted 25 October 2023
Available online 30 October 2023

of a superacid, a base or a HBD like ethylene glycol [25–27].

In the panorama of optimized DES systems for carbon capture applications, a promising low viscosity ($\eta = 110$ cP at 25 °C) CO_2 sorbent was recently developed by Ciancaleoni et al. [28] by mixing inexpensive, commercially available and safe materials, such as ethylene glycol (EG), potassium hydroxide (KOH) and boric acid (BA). The reactions involved in the formation of the DES are shown in Fig. 1.

The system with an optimized composition of EG/KOH/BA (3:1:1) has been preliminarily characterized as a Low Temperature Transition Mixture (LTTM), which differs from a DES by showing a glass transition instead of a melting point [18,29].

This LTTM also performs as a good CO_2 absorber with a net capacity of 59 g_{CO_2}/kg_{solv}, reaching 80 g_{CO_2}/kg_{solv} when CO_2 under high pressure is used. Previous DFT studies [30] showed that both BA and the deprotonated EG formed after KOH addition can participate in capturing CO_2, leading to the formation of organic carbonated species in EG/KOH/BA (3:1:1) (Fig. 2), with viable calculated energies for both absorption and desorption mechanisms. Desorption occurs under mild conditions (60 °C, 1 atm, 30 min) and is presumably ensured by the presence of BA, since it has been shown that boron species can act as catalysts for the decomposition of hydrogencarbonates [31–33].

Since the structure of a liquid strongly influences its physicochemical properties, it must be carefully studied when developing a suitable system for large-scale carbon capture. In fact, a system's viscosity depends on the magnitude and nature of its intermolecular forces, while the availability of free –OH groups and HBD-CO_2 interactions significantly affect gas solubilities. These properties can be efficiently modulated by changing the nature of the LTTM components of and strongly influence the ability to capture CO_2.

For these reasons, in this study we investigated how the addition of BA and KOH modify the very intricated hydrogen-bonding network of EG [34–38]. To do so, Near Infrared Spectroscopy (NIR) was selected as main technique, because of the possibility to separate the bands related to hydrogen bonded species in the overtone region [39]. The inhibiting effect of the strong hydrogen bonding on crystallization leading to the LTTM's glass-transition was also investigated though Differential Scanning Calorimetry (DSC). Finally, the structure of the liquid was investigated also after the absorption/desorption of CO_2 through NIR and DSC experiments.

2. Materials and methods

2.1. Materials

Ethylene glycol (≥99.8 %), potassium hydroxide (≥85 %) were purchased from Sigma-Aldrich, boric acid (≥99.9 %) was purchased from Alfa Aesar.

2.2. LTTM preparation

The EG/KOH (3:1) mixture was prepared by dissolving potassium hydroxide pellets in ethylene glycol, following the procedure previously reported by Ciancaleoni et al. [28]. To minimize water contamination, the pellets were added without being crushed, and the entire procedure was performed in inert atmosphere, under a gentle nitrogen flow. Since the reaction between potassium hydroxide (KOH) and ethylene glycol (EG) is strongly exothermic, the mixture was placed in a water bath and stirred until complete dissolution of the solid, which took approximately 2–4 h. The EG/KOH/BA (3:1:1) LTTM was prepared by adding the proper amount of boric acid to the previously prepared EG/KOH mixture until complete dissolution.

2.3. CO_2 absorption and desorption

Carbonation of the system was achieved by connecting a 25 mL round-bottom flask containing 4 g of EG/KOH/BA (3:1:1) to a 500 mL flask filled with pure CO_2 gas. The LTTM was kept under constant stirring at 900 rpm in a temperature-controlled water bath at 20 °C. For CO_2 desorption, the carbonated sample was placed in a water bath at 60 °C and stirred for 30 min, under a constant nitrogen flow (about 65×10^{-9} m^3/s). To regenerate the solvent after desorption, a few drops of water were added to replace the water lost during heating (average H_2O loss = 530 mg), until the original weight of the LTTM before absorption was restored. The amount of absorbed and desorbed gas was estimated gravimetrically with an analytical balance (±0.1 mg).

2.4. Near-Infrared and FTIR spectroscopy

NIR spectra were acquired in the 4000–10,000 cm^{-1} wavenumber range, using a Nexus 870-FTIR (Thermo-Nicolet) coupled with a Nicolet Continuum FT-IR microscope (beam splitter: CaF_2; detector: InGaAs). A Linkham THMS600 stage was used to control the sample temperature while cooling the system from 25° to −50 °C at a 10 °C/min rate. A constant flux of nitrogen was also applied on the Linkham window to avoid condensation of moisture from the surrounding atmosphere. All NIR spectra were obtained with a 4 cm^{-1} resolution, averaged over 128 scans and were reprocessed using the Kubelka-Munk model. The deconvolution of the experimental data was performed using Origin Pro 2021 using a combination of Gaussian distributions.

Attenuated total reflection Fourier-transform infrared spectroscopy (ATR-FTIR) spectra were acquired using a Thermo-Nicolet Nexus 870 FT-IR spectrophotometer (beam splitter: KBr; detector: MCT/A), in the 4000–500 cm^{-1} range. The spectra were acquired with a 4 cm^{-1} resolution and were averaged over 128 scans. The spectra before and after absorption and desorption were recorded consecutively, using the same experimental conditions.

2.5. Differential scanning calorimetry (DSC)

DSC measurements were carried out using a DSC-Q2000 (TA Instruments). The curves were acquired by heating the system with a 2 °C/min ramp from −80° to 30 °C, after a 10 min equilibration at −80 °C. The experiments were conducted in N_2 atmosphere, with a flow rate of 50 mL/min, using aluminum hermetic pans.

2.6. Computational details

All the calculations were performed with the Orca code [40] version

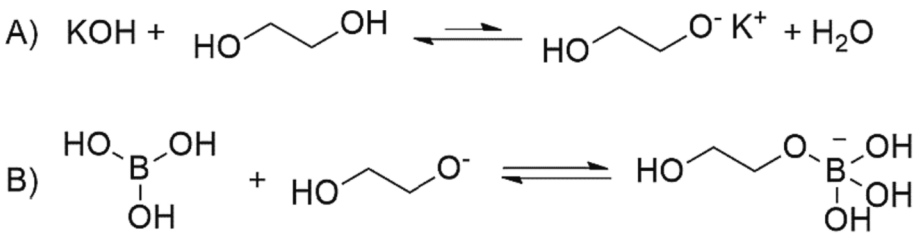

Fig. 1. Equilibria occurring in the EG/KOH/BA (3:1:1) system [28]. Scheme **A** shows the acid-base reaction between EG and KOH, while reaction **B** shows the formation of a Lewis adduct between BA and EG.

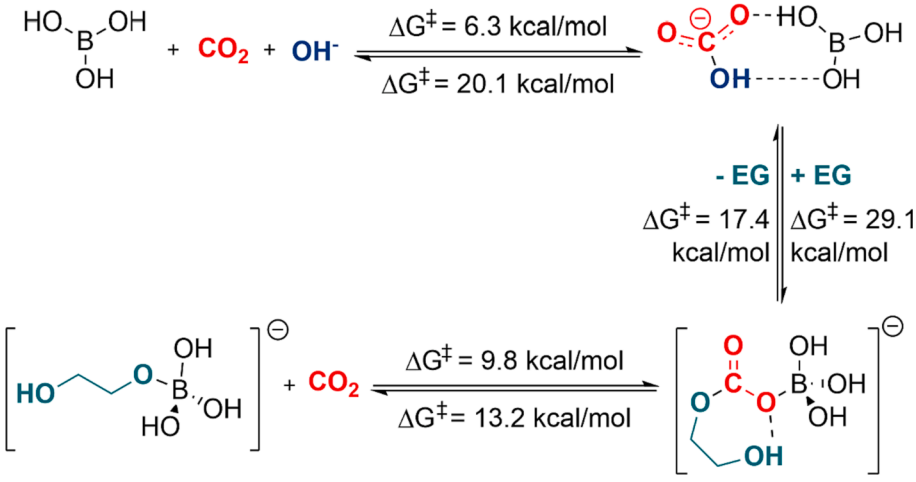

Fig. 2. Interconnected CO_2 capture mechanisms for the EG/KOH/BA (3:1:1) LTTM [30]. Adapted from Ref. 30, Copyright 2023, with permission from Elsevier.

5.0.1 [41], at the B3LYP/def2-TZVP level and def2/J auxiliary basis. Dispersion effects were taken into account using the Grimme D3-parametrized empirical dispersion correction, with the Becke–Johnson (BJ) damping function [42,43] Frequency calculations were carried out at the same level of theory, to ensure that the stationary structures had no imaginary frequencies. The solvent effects were modelled using the Conductor-Like Polarizable Continuum Model (CPCM) [44] with ethylene glycol as solvent by including its specific parameters in the calculations (dielectric constant 41.4 and refractive index 1.43).

3. Results and discussions

3.1. Molecular structure of EG/KOH (3:1)

Fig. 3 shows the spectra of EG/KOH (3:1) (in red) and pure EG (in blue). The peak assignments are listed in Table 1, together with the peak positions for pure EG.

The addition of KOH to EG causes a red shift in the C–H bending and CH_2 bending + stretching bands [45] at 4356 and 5805 cm^{-1}, respectively. On the other hand, the band at 4785 cm^{-1}, due to C–H bending and O–H stretching + bending vibrations [45], remains in the same position, albeit less intense if compared to pure EG.

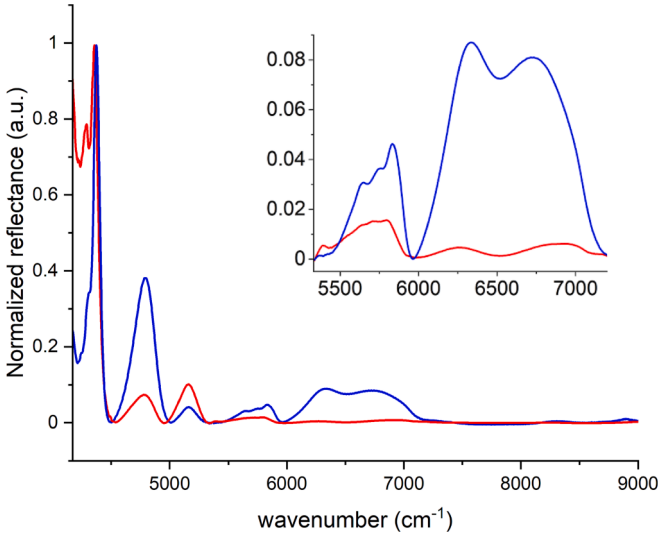

Fig. 3. NIR spectra of pure EG (blue) and EG/KOH (3:1) (red) at 25 °C, normalized with respect to the peak at 4356 cm^{-1} The inset shows a magnification of the figure to display the lower intensity peaks.

Table 1
Peak position for the main NIR peaks of EG/KOH (3:1) compared to pure EG.

Peak position in EG/KOH (cm^{-1})		Peak position in EG (cm^{-1})	Vibration	Assignment [35]
6977-6851	~6831	6701-6547	1st overtone O-H stretch ($\nu_1 + \nu_3$) of H_2O + 2ν (OH)	EG-H_2O-EG + H_2O-H_2O + EG-EG weakly bonded
	~6985			free -OH
6238		6339-6308	1st overtone O-H stretch 2ν (OH)	EG-EG strongly bonded
5805		5839	1st overtone C-H stretch	–
5150		5164-5156	O-H bend + sym. stretch of H_2O ($\nu_2 + \nu_3$)	EG-H_2O-EG + H_2O-H_2O
4785		4786	O-H and C-H bend + O-H stretch	–
4356		4375	C-H_2 bend. + stretch	–

However, this study focuses on the vibrations of hydrogen bonded species. EG has diol hydroxyl groups, which can act both as HBDs and HBAs, leading to a very intricate hydrogen-bonding network which affects the solvent's molecular structure, through the formation of EG clusters [34–38].

Following a previous work of Chen et al. [35] on ethylene glycol–water mixtures, the HBs between hydroxyl groups were investigated by considering O–H vibrations bands. The spectrum of EG/KOH (3:1) shows two main bands that originate from the O–H stretching vibrations in the 6000–7100 cm^{-1} region of the NIR spectra (Fig. 4). These bands are related to vibrations of weakly and strongly bonded –OH groups in the LTTM. The addition of KOH to EG brings about a shift in the first peak (weakly bonded –OH groups) to 6977–6851 cm^{-1} and a shift of the second peak (strongly bonded –OH) to 6238 cm^{-1}. The new peaks appear then at higher and lower energies compared to the spectrum of pure EG, respectively.

Fig. 4 shows the 6000–7100 cm^{-1} region of the spectrum of EG and EG/KOH. The figure shows that the presence of KOH also induces a sharpening and a separation of the two signals.

The band at 6977–6851 cm^{-1} in the EG/KOH sample is blue shifted compared to the band in pure EG. This shift is due to the presence of water in the system formed during the reaction between EG and KOH in the formation of the liquid LTTM (Fig. 1**A**). The increased water content is also confirmed by the increment of the $\nu_2 + \nu_3$ band at 5150 cm^{-1} relative to water and can partly explain the closeness of the 6977–6851 cm^{-1} band in EG/KOH to the position of the $\nu_1 + \nu_3$ peak in bulk water

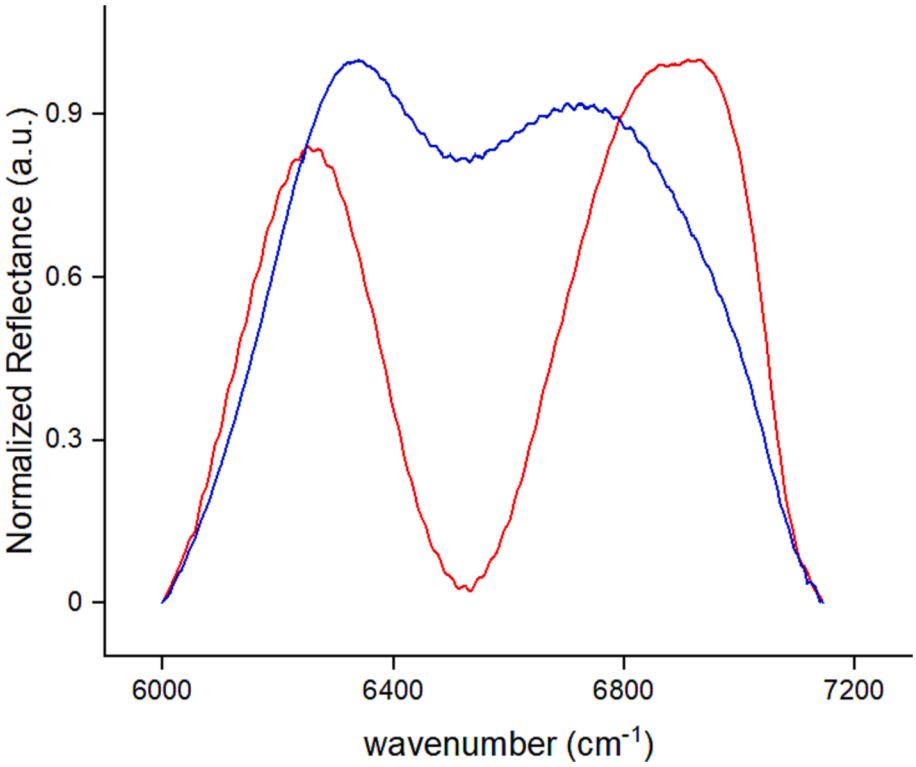

Fig. 4. O–H stretching bands for pure EG (blue) and EG/KOH (3:1) (red) at 25 °C in the 6000–7100 cm^{-1} region, normalized with respect to the peaks at 6339 cm^{-1} and 6851 cm^{-1}, respectively.

(6887 cm^{-1}) [35].

DFT studies performed on pure EG showed that in the most stable structure two EG molecules establish three intermolecular H-bonds between their –OH groups (structure EG_2(b) in **Figure S1**). This is in agreement with the literature [34,46]. The addition of a water molecule does not alter the structure of the dimer but bridges the two moieties (structures EG_2_H_2O(a)-(c), **Figure S1**). The analysis of trimers, tetramers and hexamers of EG perturbed by water shows that in general the

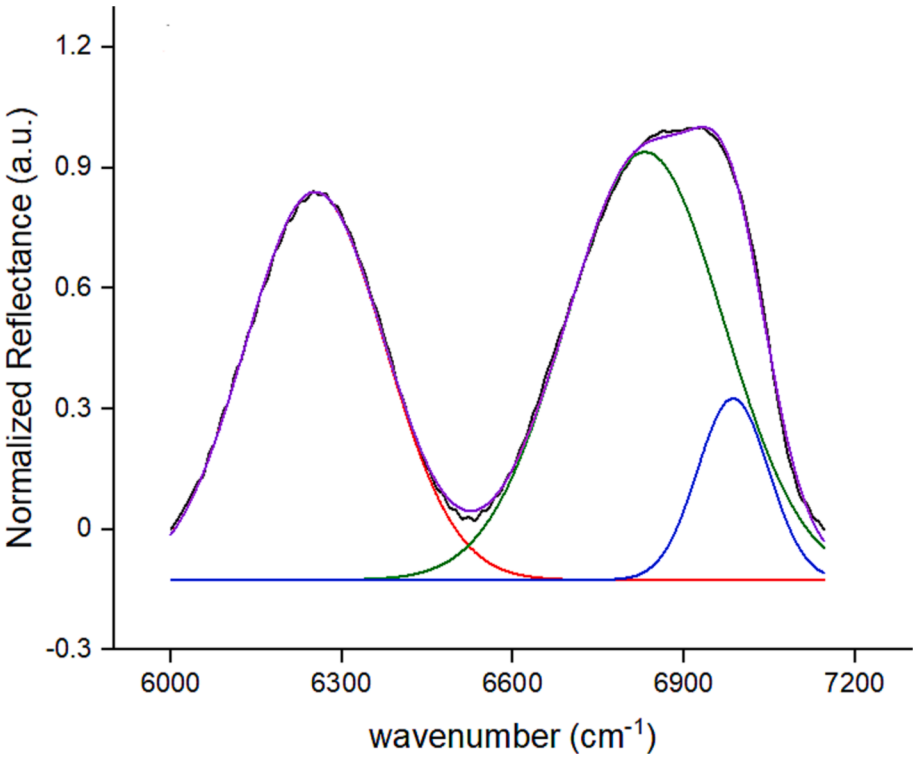

Fig. 5. Gaussian deconvolution of the 6000–7100 cm^{-1} NIR band of EG/KOH (3:1) (black) at 25 °C into its components assigned to strong EG-EG (red),EG-H_2O-EG + H_2O-H_2O(green) interactions and to free OH groups (blue)., The reconstructed overall curve obtained by the combination of the deconvoluted peaks is in purple.

geometries in which the water significantly alters the structure of the initial aggregate are less stable (**Figures S2 and S3**). The main effect of water is to slightly decrease the number of EG-EG HBs. For these reasons the large red shift of the band from 6701–6547 cm^{-1} to 6850 cm^{-1} cannot be explained by considering the amount of water formed during the reaction of EG with KOH (3:1). Indeed, the EG/H_2O ratio should be close to 1:1 to justify such a shift at room temperature [35], but it is clearly larger than 3:1.

On the other hand, the closeness of the EG/KOH band to the region of the free OH groups in EG as reported in literature [35] (7000 cm^{-1}) suggests that the added KOH intercalates in the structure of liquid EG and frees some of the hydroxyl groups from HB interactions. Therefore, the increment in free OH groups shifts the 6977–6851 cm^{-1} band to higher energies. To prove this, a Gaussian deconvolution [47] of the band was also performed, and it was resolved into three components at ~ 6238, ~6831 and at ~ 6985 cm^{-1}, respectively, as shown in Fig. 5. The contribution at about 6831 cm^{-1} can be assigned to 2 ν (OH) vibrations of weakly bonded –OH groups of EG and ($\nu_1 + \nu_3$) vibrations of H_2O engaging in EG-H_2O-EG and H_2O-H_2O interactions [35], while the component at ~ 6985 cm^{-1} can be related to the vibrations of free –OH groups, very close to the expected 7000 cm^{-1} region as reported in the literature [35].

The band at 6238 cm^{-1}, ascribed to strong EG-EG intermolecular interactions, is red shifted by about 100 cm^{-1} compared to its position in pure EG, suggesting the HB interactions between EG molecules become stronger when the LTTM forms. Computed vibrational frequencies for the O–H stretching confirmed this behaviour: when ethylene glycol molecules form a cluster, the O–H stretch associated to groups involved in HBs is found at 3293 cm^{-1}. If KOH is added to the system, the frequency is red shifted to 3162 cm^{-1}.

However, when compared to its weakly bonded and free –OH components in Fig. 4 the strong EG-EG band has a smaller contribution in terms of peak area and intensity to the overall 6000–7100 cm^{-1} region for EG/KOH (3:1). Presumably EG-H_2O-EG and H_2O-H_2O interactions prevail over EG-EG interactions at room temperature when KOH is present. This behaviour is opposite to what was observed for pure EG, where intermolecular interactions between diol molecules are predominant [35] and provides further confirmation of the disruption induced by KOH on the solvent structure.

The effect of temperature on the HB network was evaluated by recording the spectral changes at different temperatures, from −50° to 25 °C (**Figure S4**). All bands show an increase in intensity and peak area upon cooling, suggesting an overall reinforcement of the intermolecular interactions. Interestingly, for the EG/KOH (3:1) LTTM the band at 6977–6851 cm^{-1} shows a blue shift of 120 cm^{-1} (**Figure S5C**) when the temperature drops from 25 °C to −5 °C, suggesting an increase in the free –OH contribution at lower temperatures. EG exhibits the opposite behaviour, with a significant red shift (154 cm^{-1}) between −10 °C and −20 °C for the same band (**Figure S6**). For EG/KOH, the plot of the peak intensity as a function of temperature (**Figure S5A**) exhibits a change in the slope at approximately −25 °C, indicating a molecular rearrangement of the liquid structure. The position of the peak at 6238 cm^{-1} remains unaltered upon cooling, while the peak intensity increases to a slightly higher extent compared to the $\nu_1 + \nu_3$ band (**Figure S7**).

The presence of several free –OH groups in the EG/KOH (3:1) LTTM, as suggested by the analysis of the NIR spectra, explains the high values of irreversible CO_2 absorption reported by Ciancaleoni et al. [28]. Since these hydroxyl groups are not engaged in HB, they can easily capture the gas through the formation of potassium hydrogencarbonate and carbonated EG, up to 140 g_{CO_2}/kg_{solv} [35].

3.2. Molecular structure of EG/KOH/BA (3:1:1)

Fig. 6 shows the spectrum of EG/KOH/BA (3:1:1) compared to EG/KOH (3:1). The assignments for the main peaks are reported in Table 2, compared to those in EG/KOH.

The NIR spectrum of EG/KOH/BA (3:1:1) shows a very sharp and intense peak at 4377 cm^{-1}, that overlaps with a smaller peak at 4314 cm^{-1}. These components are assigned to C-H_2 bending + stretching vibrations. The peak at 4377 cm^{-1} is blue shifted from its position in EG/

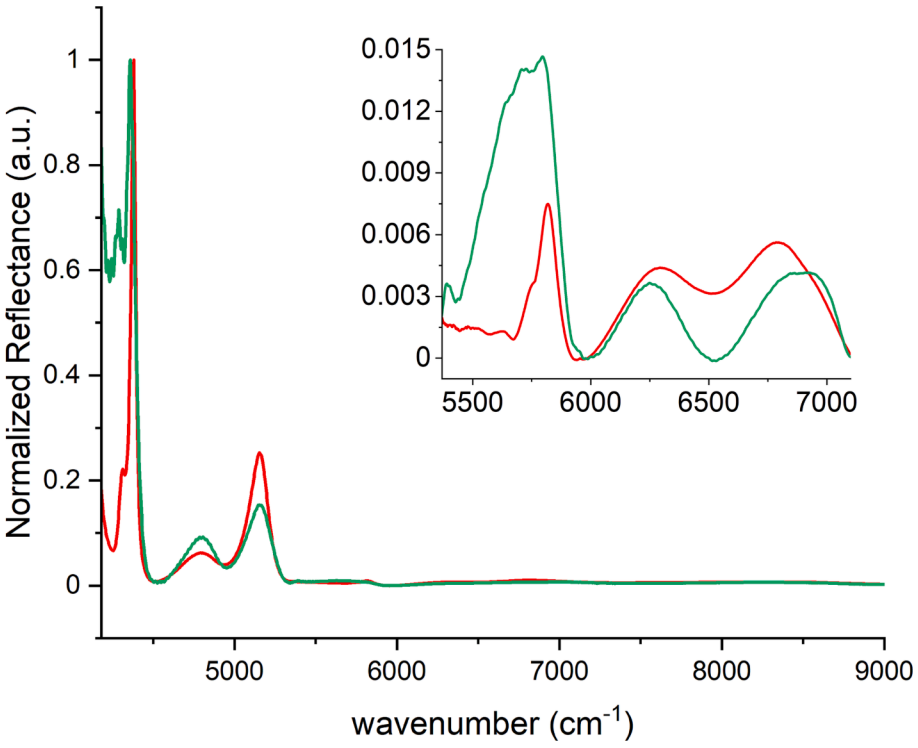

Fig. 6. NIR spectra of EG/KOH/BA (3:1:1) (red) and EG/KOH (3:1) (green) at 25 °C, normalized with respect to the intensity of the signal at 4377 and 4356 cm^{-1}. The inset shows lower intensity peaks.

Table 2
Peak positions for the main NIR peaks of EG/KOH/BA (3:1:1) compared to EG/KOH (3:1).

Peak position in EG/KOH/BA (cm^{-1})	Peak position in EG/KOH (cm^{-1})	Vibration	Assignment [35]
6790-6736	6977-6851	1st overtone O-H stretch ($\nu_1 + \nu_3$)	EG-H_2O-EG + H_2O- H_2O
6273-6250	6238	1st overtone O-H stretch	EG-EG strongly bonded
5814-5808	5805	1st overtone C-H stretch	–
5151-5143	5151	O-H bend + sym. stretch in H_2O ($\nu_2 + \nu_3$)	EG-H_2O-EG + H_2O- H_2O
4784-4763	4785	O-H and C-H bend + O-H stretch	–
4314	–	C-H_2 bend. + stretch	–
4377	4356	C-H_2 bend. + stretch	–

KOH (3:1). The broad band at 4784–4763 cm^{-1} is assigned to a combination of C–H bending and O–H bending + stretching vibrations. This band is less intense than the corresponding peak in EG/KOH (3:1) and is located at lower wavenumbers.

The 6000–7100 cm^{-1} region of the NIR spectrum, relative to the first overtone of O–H stretching vibrations, reflects the addition of BA to EG/KOH (3:1) and the perturbation it produces on the H-bonding. The spectral differences of EG/KOH/BA (3:1:1) and EG/KOH (3:1) in this region are shown in Fig. 7.

The addition of BA induces a shift of the band relative to weakly bonded OH groups to lower energies. In EG/KOH/BA (3:1:1) this band is located at 6790–6736 cm^{-1}, that corresponds to a shift of approximately 190 cm^{-1} from the 6977–6851 cm^{-1} region that was found for the EG/KOH (3:1) sample. This large shift can be ascribed to an important decrease in the free OH component, due to the formation of a Lewis adduct between EG and BA through the EG free hydroxyl groups (Fig. 1**B**). The peak broadening and shift to lower energies also suggest a simultaneous reinforcement of EG-H_2O-EG and H_2O-H_2O interactions, which is consistent with the reduction in the free OH population.

The peak at 6273–6250 cm^{-1}, due to strong EG-EG interactions, is located at higher wavenumbers if compared to the same band in EG/KOH (3:1). This behaviour is confirmed by computed vibrations: starting from the EG/KOH system, the addition of H_3BO_3, induces a shift in the O–H stretching of strongly bonded EGs from 3162 cm^{-1} to 3222 cm^{-1} (EG_3_BA_OH). The intermolecular interactions between EG molecules are weakened by BA, presumably because of the formation of the Lewis adduct between the hydroxyl anion and boric acid. However, this peak is still located at lower energies if compared to pure EG (6339–6308 cm^{-1}). We argue that EG-EG interactions are still stronger in the LTTM respect to pure EG. The predominant contribution of EG-H_2O-EG and H_2O-H_2O components to the overall band in the 6000–7100 cm^{-1} region shown in Fig. 7 indicates that the interactions between EG and H_2O prevail over the strong EG-EG interactions at room temperature, as previously seen for EG/KOH (3:1). In this case however, the EG-water interactions became stronger upon addition of BA.

Fig. 8 shows the NIR bands of EG/KOH/BA (3:1:1) in the first overtone region of OH stretching vibrations recorded between 25 °C and −50 °C. Temperature dependencies of both bands show a shift towards lower wavenumbers in the cooling ramp, indicating a reinforcement of all the corresponding intermolecular forces. Passing from 25 to −50 °C the intensity and the area under the peak of the 6273–6250 cm^{-1} band show a steeper increase compared to the weakly bonded OH component. This implies that at low temperatures the EG-EG contribution becomes predominant over EG-water interactions, which is the opposite of what occurs at room temperature. Furthermore, an isosbestic point [48] at around 6930 cm^{-1} indicates a reduction in the free OH population upon cooling. Interestingly, the peak intensity plots as a function of temperature (**Figure S9A and S10A**) exhibit a step-like discontinuity between −27.5 °C and −30 °C for both bands, suggesting a structural rearrangement in this range.

To further investigate the effect of temperature on the molecular structure, DSC measurements were performed (**Figure S11**). The thermograms show a glass transition at T_g = -42 °C for the EG/KOH/BA (3:1:1) sample. This occurring confirms that the EG/KOH/BA (3:1:1) mixture has a glass-forming behaviour and is an LTTM. This is likely due to the strong intermolecular interactions, that hamper crystallization at low temperatures [20]. The sudden spectral changes recorded when dropping the temperature below −25 °C (Fig. 8), could thus be explained by the molecular rearrangement of the solvent when the system is approaching its glass transition temperature. DSC measurements also indicate that the addition of BA has a critical effect on the molecular structure of the system. For EG/KOH (3:1) an endothermic peak is observed at −71 °C, while after the BA addition the endothermic signal disappears, and a glass transition occurs, confirming that a LTTM

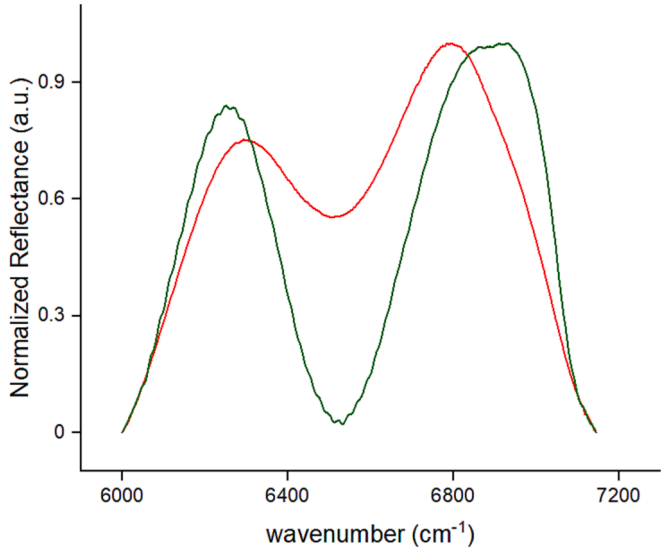

Fig. 7. EG/KOH/BA (3:1:1) (red) and EG/KOH (3:1) (green) NIR spectra in the first overtone region of O–H stretching vibrations (6000–7100 cm^{-1}) at 25 °C, normalized with respect to the peaks at 6790 and 6850 cm^{-1}.

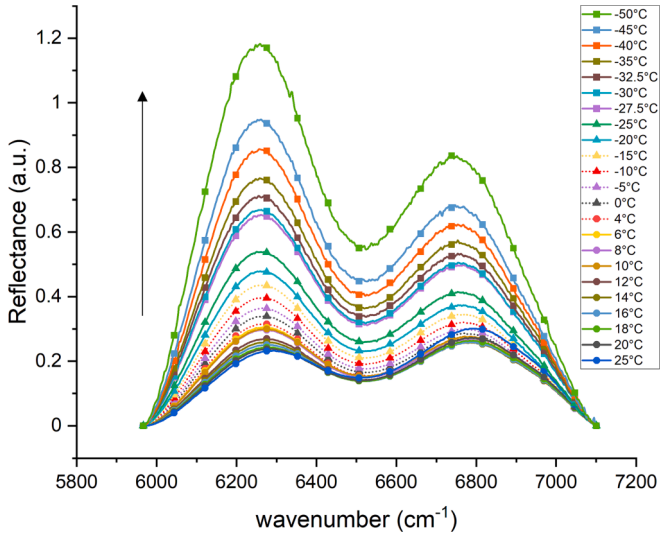

Fig. 8. First overtone region for OH stretching vibrations in EG/KOH/BA (3:1:1) NIR spectra at different temperatures, recorded between 25 °C and −50 °C. The arrow points in the direction of decreasing temperatures.

is formed.

3.3. Effects of the physico-chemical properties of LTTM on CO_2 absorption

As anticipated in the Introduction, intermolecular interactions in Deep Eutectic Solvents (DES) and Low Transition Temperature Mixtures (LTTM) have a crucial impact on their physico-chemical properties, e.g. on viscosity, melting point depression, glass forming ability and tunability. In particular, in carbon capture processes, viscosity plays a key role in CO_2 absorption, modulating the molecular exchange at the gas–liquid interface.

As reported by Ciancaleoni et al. in a previous work, in the EG/KOH (3:1) system the presence of EG acting as an HBD and the intrinsic water content due to the reaction between KOH and EG, result in a relatively low viscosity, 330 cP at room temperature [28]. This value is further lowered upon addition of BA in the EG/KOH/BA (3:1:1) LTTM, leading to a viscosity of 110 cP [28].

The absorption properties of EG/KOH/BA were assessed by measuring the amount of captured gas in different conditions.

At room temperature (20 °C), The EG/KOH/BA (3:1:1) mixture absorbs 22 ± 1 g_{CO_2}/kg_{solv} after 30 mins and 31 ± 2 g_{CO_2}/kg_{solv} after 60 mins, with an apparent plateau (Fig. 9). At 0 °C the same value is reached after 150 mins, indication that kinetics plays a significant role in the absorption process. The temperature increase to 30 °C led to an increase in absorption. In fact, the CO_2 uptake at 30 °C is 20 ± 1 and 42 ± 1 g_{CO_2}/kg_{solv} after 0.5 and 2 h, respectively. However, further heating of the system to 40 °C results in a decrease in the gas uptake. At higher temperatures the absorption efficiency decreases down to 35 g_{CO_2}/kg_{solv} after 2 h.

This apparently weird behaviour can be explained considering that the observed absorption value is not the thermodynamic value (maximum capacity), but it is likely due to the viscosity of the solvent, which limits the gas/liquid contact and the diffusion within the liquid, with the consequence of a severe slowing-down of the absorption process. This implies the non-applicability of the Henry's law. By increasing the temperature, the viscosity decreases, allowing both better contact and diffusion and, therefore, the kinetics of CO_2 absorption increases, leading to a higher value. At 40 °C, the absorption capacity decreases, likely due to a lower CO_2 solubility in the system. Notably, 60 °C are reported as the desorption temperature [28].

In order to shed more light on this phenomenon, it would be interesting to correlate the influence of the temperature on the absorption capacity and kinetics to the temperature-dependent structural changes discussed in the previous section. The increase in intensity of the strongly bonded OH band, which prevails over to weakly bonded OH band when decreasing the temperature from 25 °C, and the isosbestic point at 6930 cm^{-1} in Fig. 8 suggests a lower availability of weakly bonded free OH groups. This could explain the lower absorption at cooler temperatures, since the more strongly bonded OH groups would be less free to interact with CO_2 to form the carbonated species. Indeed, it should be remembered that the absorption is mostly due to a chemical reaction, [28,30] not to the physical dissolution of CO_2 in the LTTM.

From these considerations it can be confirmed that the rate-limiting factor is the contact of the solvent with the gas. Stirring rate and flask shape have a strong influence on the kinetics of CO_2 absorption because they modify the gas-solvent interface, while the solvent viscosity affects the diffusion of the absorbed gas in the bulk. As a matter of fact, CO_2 absorption can be further improved by adding some equivalents of water, which decreases the viscosity of the system [28].

3.4. Effect of CO_2 absorption on the structure

Fig. 10 shows the spectra of EG/KOH/BA (3:1:1) before and after the absorption of CO_2. The assignments for the main peaks are reported in Table 3.

The CO_2 uptake is confirmed by the appearance of two new bands in the 4200 cm^{-1} region (4185 and 4223 cm^{-1}), that can be ascribed to the asymmetric stretching in carbonates [49,50]. The broad band at 5806 cm^{-1}, relative to C–H stretching vibrations, is not shifted upon carbonation. Assuming the formation of the carbonated EG species proposed in Fig. 2 after CO_2 absorption, the observed increase in its

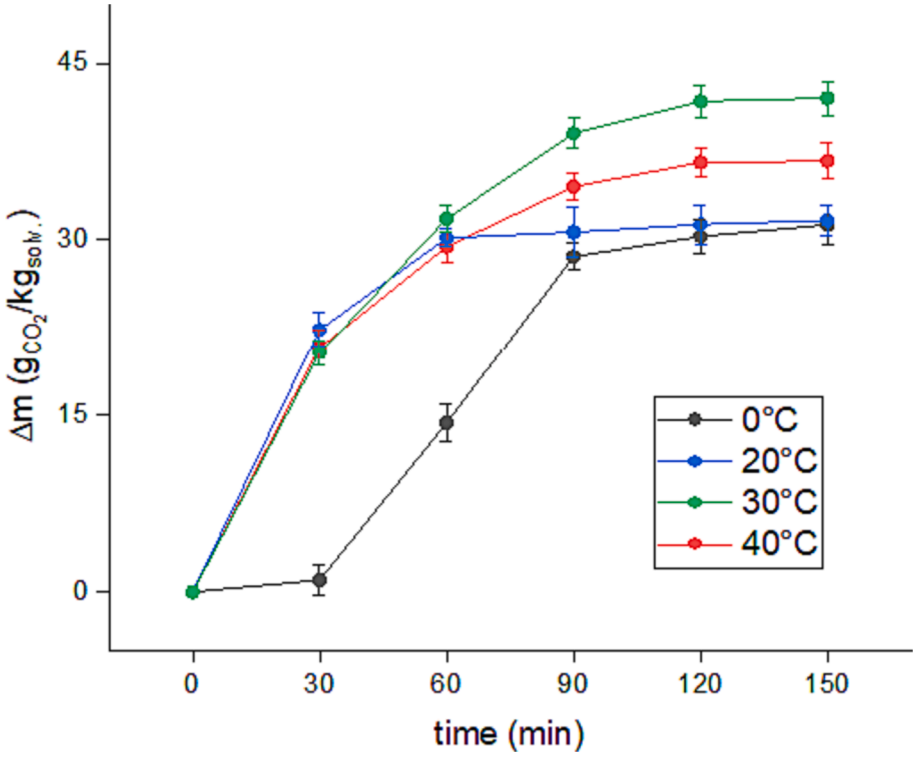

Fig. 9. CO_2 absorption over time at 0 °C (black), 20 °C (red), 30 °C (blue) and 40 °C (green) for the pure CO_2 flask system.

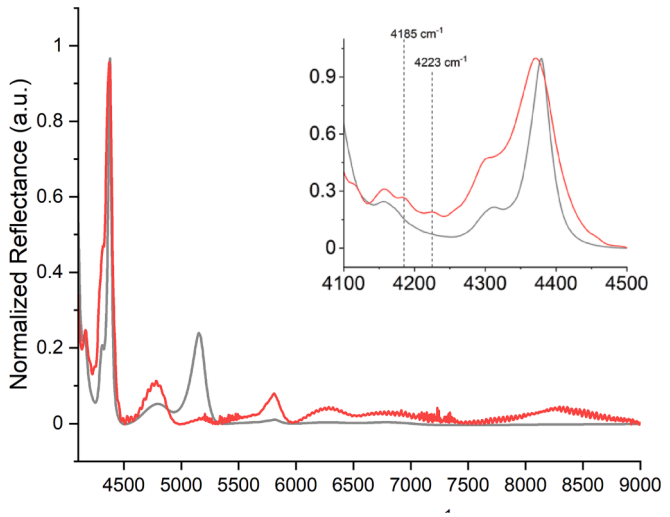

Fig. 10. NIR spectra of EG/KOH/BA (3:1:1) before (grey) and after (red) CO_2 absorption recorded at 25 °C, normalized with respect to the peaks at 4377 and 4370 cm^{-1}. The inset shows the magnification of the spectra in the 4100–4500 cm^{-1} region. The peaks at 4185 and 4223 cm^{-1} are marked with dotted lines.

Table 3
Main NIR peak assignments for EG/KOH/BA (3:1:1) after and before CO_2 absorption.

EG/KOH/BA + CO_2 (cm^{-1})	EG/KOH/BA (cm^{-1})	Vibration	Assignment [35]
6761-6736	6790-6736	1st overtone O-H stretch ($\nu_1 + \nu_3$)	EG-H_2O-EG H_2O- H_2O
6283	6273-6250	1st overtone O-H stretch	EG-EG strongly bonded
5806	5814-5808	1st overtone C-H stretch	–
5156	5151-5143	O-H bend + sym. stretch in H_2O ($\nu_2 + \nu_3$)	EG-H_2O-EG H_2O- H_2O
4780	4784-4763	O-H and C-H bend + O-H stretch	–
4302	4314	C-H_2 bend. + stretch	–
4370	4377	C-H_2 bend. + stretch	–
4223	–	CO_3 asy. Stretch.	–
4185	–	CO_3 asy. Stretch.	–
4158	4159	C-H_2 wag. + rock	–

intensity can be related to the overlap with the second overtone of C = O stretching vibrations. For esters, these vibrations give rise to a band in the 5810 cm^{-1} region [51,52]. Since little information is available on NIR band assignments for organic carbonates in the existing literature, we assume that the C = O functionality in carbonated EG is similar to that in esters.

The band at 4780 cm^{-1} is due to C–H bending and O–H bending and stretching vibrations, and is located at the same wavenumber as before carbonation. Also in this case the increase in intensity can be related to the overlap with another overtone of C = O stretching vibrations, which falls near 4900 cm^{-1} in esters [52,53]. The two bands at 4314 and 4377 cm^{-1} are assigned to C-H_2 bending and stretching vibrations, both red shifted compared to their position before the absorption of CO_2.

NIR spectra of carbonated EG/KOH/BA (3:1:1) show a band at 6761–6736 cm^{-1}, due to EG-H_2O-EG interactions. The weakly bonded OH band is located at lower wavenumbers compared to its position before carbonation. This red shift can be explained by invoking a decrease in the free OH component, due to the reaction between EG and CO_2. Moreover, the red shift suggests a strengthening in the EG-H_2O-EG interactions.

The band at 6283 cm^{-1}, due to EG-EG interactions, is blue shifted compared to its position in the LTTM before CO_2 capture, suggesting that the interactions between EG molecules are weakened by the formation of the carbonate species. The OH groups of EG react with CO_2 to give carbonated EG, leading to a decrease in the available hydroxyl groups engaged in H-bonding interactions. Indeed, also the computational analyses support this effect: when CO_2 is absorbed, the computed O–H stretch of bound EGs increases from 3222 (EG_3_BA_OH) to 3287 and 3301 cm^{-1} (EG_3_CO_2_BA).

Finally, the peak at 5156 cm^{-1}, due to the $\nu_2 + \nu_3$ vibrations of water and to H_2O-H_2O and EG-H_2O-EG interactions, is slightly blue shifted, due to the reduced availability of EG's OH groups, as discussed above.

The peak area and intensity of the 6761–6736 cm^{-1} band depend on temperature (**Figure S12**), in fact both parameters increase as temperature decreases, with a change in the slope around −25 °C, as seen before for both EG/KOH and EG/KOH/BA, and show a step-like trend between −30° and −35 °C. An overall blue shift of 25 cm^{-1} upon temperature decrease is observed. This behaviour is opposite to what we observed for the EG/KOH/BA (3:1:1) sample prior to CO_2 addition. The shift of the band towards higher energies indicates a weakening in the EG-water intermolecular interactions upon cooling. On the other hand, the positions of the 6283 cm^{-1} and 5156 cm^{-1} bands are not affected by temperature variations, even if they exhibit the same trends as the $\nu_1 + \nu_3$ band for peak area and intensity (**Figures S13 and S14**).

These results suggest that carbonation has a remarkable effect on the system's molecular structure, affecting EG-EG and EG-H_2O-EG interactions. DSC measurements show that the glass transition temperature T_g is lowered by carbonation, passing from −42° to −58 °C (**Figure S11**). This behaviour indicates that the molecular rearrangements induced by cooling can be hampered by CO_2 capture. This is consistent with the weakening of the intermolecular interactions at lower temperature suggested by the red shift observed for the weakly bonded OH band.

3.5. Solvent regeneration after desorption

Heating the carbonated system at 60 °C results in an average weight loss of 13.3 % after absorption, and 13.6 % of the initial weight of the LTTM (**Figure S15**). Previous TGA measurements on the same system (see the Supplementary Information in ref. 28) showed that during the heating up to 275 °C excess water and some EG are lost by the sample, together with CO_2. This causes a significant change in the viscosity of the liquid. The mixture reverts to its original state upon re-addition of excess water, at least for 10 cycles.

The contribution of CO_2 release during heating to the total weight loss was proved by means of ^{13}C NMR spectroscopy, which showed a decrease in the intensity of the peaks at 160.47 and 158.39 ppm, as reported by Ciancaleoni et al. (see Fig. 5 in Ref. 28).

Fig. 11 shows the ATR-FTIR spectra of EG/KOH/BA (3:1:1) recorded before and after carbonation, and after the heat induced gas release. **Table S3** reports the ATR-FTIR peak assignments before and after CO_2 absorption. A confirmation of effective CO_2 desorption is provided by the spectral changes in the ATR-FTIR spectrum of the system after heating. The system exhibits the same bands as EG/KOH/BA (3:1:1) before desorption, located at the same positions. The two spectra recorded before and after CO_2 release overlap almost perfectly, except for some spectral differences in the 1150–1800 cm^{-1} region, as shown in the inset of Fig. 11.

The almost perfect overlap of the initial spectrum with those recorded for the carbonated system before and after desorption (**Table S3**) suggests that CO_2 capture and release do not significantly perturbate the system, as all significant spectral changes can be exclusively ascribed to the presence of organic carbonates.

The vibrations of organic carbonates are located in the 1150–1800 cm^{-1} region: they typically show an intense band at 1205–1280 cm^{-1} due to O-C-O asymmetric stretching vibrations, accompanied by a second intense band at 1740 cm^{-1} due to C = O stretching [53]. The band at

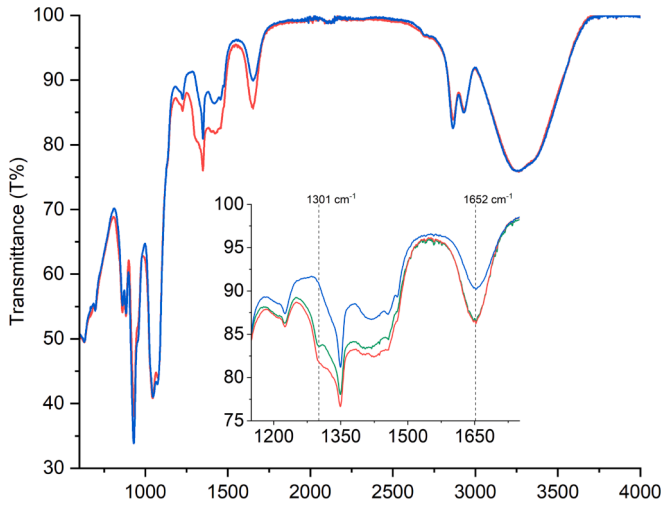

Fig. 11. ATR-FTIR spectra for EG/KOH/BA (3:1:1) before (blue) and after (red) absorption, and after desorption (green). The inset shows the magnification of the spectra in the 1150–1700 cm^{-1} region. The peaks at 1301 and 1652 cm^{-1} are marked with dotted lines.

1297–1301 cm^{-1} was not present in the LTTM before carbonation and can be assigned to O-C-O asymmetric stretching vibrations, although located at higher energies. The proximity of the carbonate moiety to the borate functionality in the Lewis adduct reported in Fig. 2 explains the reason why the band is shifted to higher energies.

Similarly, the increased peak intensity at 1652 cm^{-1} in the system after absorption can be related to the presence of organic carbonated species instead of increased H_2O concentrations due to moisture absorption. The increase in force constant and stretching frequency of the O-C-O bond in carbonated EG result in a decrease of its C = O stretching energy [53]. Thus, the C = O stretching band can fall in the same region as O-H_2 bending vibrations, determining an increase in peak intensity at 1652 cm^{-1} after carbon capture. These findings agree with the results obtained by Chen et al. [54] for FTIR measurements on an EG-superbase DES after CO_2 capture, which showed the appearance of a peak at 1263 cm^{-1} and an increase in the peak at 1649 cm^{-1}.

From the inset in Fig. 11 we argue that the O-C-O asymmetric stretching band at 1301 cm^{-1} shows a decrease in both area and intensity after heating at 60 °C, while it becomes less broad and slightly shifted (4 cm^{-1}). The peak narrowing can indicate a partial CO_2 release during desorption. Desorption is not complete since the peak does not disappear after heating: its shift suggests that multiple carbonate species contribute to the overall band, and one or more species remain in the system at higher amounts after desorption. Anyway, this does not hamper the possibility to perform multiple absorption/desorption cycles, as already reported [28].

4. Conclusions and perspectives.

In this work, NIR measurements showed how the intricate interplay of intermolecular interactions in the EG/KOH/BA (3:1:1) LTTM affects the delicate equilibrium between the system physico-chemical properties and an effective CO_2 absorption. The relationship between the LTTM's molecular structure and its ability to capture the gas were investigated, paving the way to a better understanding of desired LTTM properties for developing viable carbon capture systems.

We found that temperature plays a key role in gas absorption, strongly influencing the H-bonding network of the system and therefore its viscosity and the molecular exchange at the gas-solvent interface during mixing, but especially the availability of weakly bonded and free OH groups which ensured effective CO_2 capture through organic carbonate formation, leading to an average absorption of 22 ± 1 g_{CO_2}/kg_{solv} at room temperature. The presence of BA, acting as a catalyst for the carbonate decomposition, ensured CO_2 release at 60 °C and the recyclability of the system over multiple absorption/desorption cycles.

Although the gas release is not 100 % complete during desorption, ATR-FTIR measurements proved the solvent is mostly regenerated after desorption and can thus continue to absorb further CO_2 over a large number of cycles, making the system reusable.

The role of water in the formation and performance of this LTTM system is an interesting issue that deserves more attention in future upcoming studies. In fact, while water competes with CO_2 for the absorption sites and can decrease the capturing efficiency [23,24], however it also decreases the viscosity of the LTTM, which promotes the absorption of carbon dioxide, and perturbs the set of hydrogen bonds in the EG/KOH/BA structure.

CRediT authorship contribution statement

Tanja Traini: Investigation, Methodology, Validation, Writing – original draft, Writing – review & editing. **Duccio Tatini:** Investigation, Data curation, Writing – original draft, Writing – review & editing. **Elisa Rossi:** Investigation, Software, Writing – original draft, Writing – review & editing. **Gianluca Ciancaleoni:** Conceptualization, Supervision, Resources, Writing – original draft, Writing – review & editing. **Pierandrea Lo Nostro:** Conceptualization, Supervision, Funding acquisition, Resources, Writing – original draft, Writing – review & editing.

Declaration of Competing Interest

The authors declare that they have no known competing financial interests or personal relationships that could have appeared to influence the work reported in this paper.

Data availability

Data will be made available on request.

Appendix A. Supplementary data

Supplementary data to this article can be found online at https://doi.org/10.1016/j.molliq.2023.123441.

References

[1] United Nations, Framework Convention on Climate Change, Adoption of the Paris Agreement, 21st Conference of the Parties, Paris, 2015.
[2] Working Group III of the IPCC, IPCC Special Report on Carbon Dioxide Capture and Storage, Cambridge Univ. Press, 2005.
[3] IPCC; Climate Change 2007: Synthesis Report, Contribution of Working Groups I, II and III to the Fourth Assessment Report of the Intergovernmental Panel on Climate Change, IPCC, Geneva, Switzerland, 2007.
[4] M. Meinshausen, N. Meinshausen, W. Hare, S.C.B. Raper, K. Frieler, R. Knutti, D. J. Frame, M.R. Allen, Greenhouse-gas Emission Targets for Limiting Global Warming to 2°C, Nature 458 (2009) 1158–1162.
[5] M. Bui, C.S. Adjiman, A. Bardow, E.J. Anthony, A. Boston, S. Brown, P.S. Fennell, S. Fuss, A. Galindo, L.A. Hackett, J.P. Hallett, H.J. Herzog, G. Jackson, J. Kemper, S. Krevor, G.C. Maitland, M. Matuszewski, I.S. Metcalfe, C. Petit, G. Puxty, J. Reimer, D.M. Reiner, E.S. Rubin, S.A. Scott, N. Shah, B. Smit, J.P.M. Trusler, P. Webley, J. Wilcox, N. Mac Dowell, Carbon Capture and Storage (CCS): The Way Forward, Energy Environm. Sci. 11 (5) (2018) 1062–1176.
[6] A.B. Klass, E.J. Wilson, Climate Change and Carbon Sequestration: Assessing a Liability Regime for Long-Term Storage of Carbon Dioxide, Emory Law J. 58 (2008).
[7] B. Dutcher, M. Fan, A.G. Russel, Amine-Based CO_2 Capture Technology Technology Development from The Beginning of 2013. ACS Appl. Mater. Interfaces 7 (2015) 2137-2148.
[8] M. Vaccarelli, P. Carapellucci, L. Giordano, Energy and Economic Analysis of the CO_2 Capture from Flue Gas of Combined Cycle Power Plants, Energy Procedia 45 (2014) 1165–1174.
[9] L.A. Kohl, R. Nielsen, Gas Purification, 5th Edition, Gulf Publishing Company, Houston, Texas, 1997.

[10] S.A. Didas, R. Zhu, N.A. Brunelli, D.S. Sholl, C.W. Jones, Thermal, Oxidative and CO_2 Induced Degradation of Primary Amines Used for CO_2 Capture: Effect of Alkyl Linker on Stability, J. Phys Chem. 118 (2014) 12302–12311.
[11] B.B. Hansen, S. Spittle, B. Chen, B. Chen, D. Poe, Y. Zhang, J.M. Klein, A. Horton, L. Adhikari, T. Zelovich, B.W. Doherty, B. Gurkan, E.J. Maginn, A. Ragauskas, M. Dadmun, T.A. Zawodzinsky, G.A. Baker, M.E. Tuckerman, R.F. Savinell, J. R. Sangoro, Deep Eutectic Solvents: A Review of Fundamentals and Applications, Chem. Rev. 121 (2021) 1232–1285.
[12] P. Anastas, J.G. Warner, Green Chemistry Theory and Practice, Oxford University Press, New York, 1998.
[13] A.P. Abbott, G. Capper, D.L. Davies, R.K. Rasheed, V. Tambyrajah, Novel Solvent Properties of Choline Chloride Urea Mixtures, Chem. Commun. (2003) 70–71.
[14] R.D. Rogers, K.R. Seddon, Ionic Liquids: Industrial Applications for Green Chemistry, Oxford University Press, Oxford, 2002.
[15] A.P. Abbott, D. Boothby, G. Capper, D.L. Davies, R.K. Rasheed, Deep Eutectic Solvents Formed between Choline Chloride and Carboxylic Acids: Versatile Alternatives to Ionic Liquids, J. Am. Chem. Soc. 126 (2004) 9142–9147.
[16] P. Xu, G.W. Zheng, M.H. Zong, N. Li, W.Y. Lou, Recent Progress on Deep Eutectic Solvents in Biocatalysis, Bioresour. Bioprocess. 4 (2017) 34.
[17] S. Khandelwal, Y.K. Tailor, M. Kumar, Deep Eutectic Solvents (DESs) as Eco-friendly and Sustainable Solvent/Catalyst Systems in Organic Transformations, J. Mol. Liq. 215 (2016) 345–386.
[18] M. Francisco, A. Van der Bruinhorst, M.C. Kroon, Low Transition-Temperature Mixtures (LTTMs): A New Generation of Designer Solvents, Angew. Chem. 52 (2013) 3074–3085.
[19] L.J.B.M. Kollau, M. Vis, A. van den Bruinhorst, A.C.C. Esteves, R. Tuinier, Quantification of the Liquid Window of Deep Eutectic Solvents, Chem. Commun. 54 (95) (2018) 13351–13354.
[20] A.P. Abbott, R.C. Harris, K.S. Ryder, Applications of Hole Theory to Define Ionic Liquids by their Transport Properties, J. Phys. Chem. B 111 (2007) 4910–4913.
[21] D.V. Wagle, H. Zhao, G. Baker, Deep Eutectic Solvents: Sustainable Media for Nanoscale and Functional Materials, Acc. Chem. Res. 47 (2014) 2299–2308.
[22] B. Tang, K.H. Row, Recent Developments in Chemical Sciences, Montash. Chem. 144 (2013) 1427–1454.
[23] S. Aparicio, M. Athilhan, Water Effect on CO_2 Absorption for Hydroxylammonium Based Ionic Liquids: A Molecular Dynamics Study, Chem. Phys. 400 (2012) 118–125.
[24] W.C. Su, D.S.H. Wong, M.H. Li, Effect of Water on Solubility of Carbon Dioxide in (Aminomethanamide + 2-Hydroxy-N, N, N-Trimethylethanaminium Chloride), J. Chem. Eng. Data 54 (6) (2009) 1951–1955.
[25] Y. Hou, Y. Gu, S. Zhang, F. Yang, H. Ding, Y. Shan, Novel Binary Eutectic Mixtures Based on Imidazole, J. Mol. Liq. 143 (2-3) (2008) 154–159.
[26] P.A. Bhawna, S. Pandey, Superbase-Added Choline Chloride-Based Deep Eutectic Solvents for CO_2 Capture and Sequestration, Chemistry Select. 2 (2017) 11422–11430.
[27] C. Florindo, F.S. Oliveira, L.P.N. Rebelo, A.M. Fernandes, I.M. Marrucho, Insights into the Synthesis and Properties of Deep Eutectic Solvents Based on Cholinium Chloride and Carboxylic Acids, ACS Sustainable Chem. Eng. 2 (10) (2014) 2416–2425.
[28] M. Costamagna, E. Micheli, V. Canale, M. Ciulla, G. Siani, P. di Profio, M. Tiecco, G. Ciancaleoni, Low-Cost Temperature Transition Mixtures (TTM) Based on Ethylene Glycol/Potassium Hydroxide as Reversible CO_2 Sorbents, J. Mol. Liq. 340 (2021), 117180.
[29] H. Ghaedi, M. Ayoub, S. Sufian, A.M. Shariff, B. Lal, C.D. Wilfred, Density and Refractive Index Measurements of Transition-Temperature Mixture (Deep Eutectic Analogues) Based on Potassium Carbonate with Dual Hydrogen Bond Donors for CO2 Capture, J. Chem. Thermodyn. 118 (2018) 147–158.
[30] E. Rossi, G. Ciancaleoni, Theoretical Insights into the Reversible CO2 Absorption by Ethylene Glycol/KOH/Boric Acid Low Temperature Transition Mixture, J. Mol. Liq. 381 (2023), 121843.
[31] L. Lombardo, H. Yang, P.J. Zhao, P.J. Dyson, A. Zuttel, Solvent- and Catalyst-Free Carbon Dioxide Capture and Reduction of Formate with Borohydride Ionic Liquids, Chem. Sus. Chem. 13 (2020) 2025–2031.
[32] A. Filippov, O.N. Antzutkin, F.U. Shah, Understanding the Interaction of Boric Acid and CO_2 with Ionic Liquids in Aqueous Mediums by Multinuclear NMR Spectroscopy, ACS Sustain. Chem. Eng. 8 (2020) 552–560.
[33] D. Guo, H. Thee, G. da Silva, J. Chen, W. Fei, S. Kentish, G.W. Stevens, Borate-Catalyzed Carbon Dioxide Hydration via the Carbonic Anhydrase Mechanism, Environ. Sci. Technol. 45 (11) (2011) 4802–4807.
[34] R.M. Kumar, P. Baskar, K. Balamurugan, S. Das, V. Subramanian, On the Perturbation of the H-Bonding Interaction in Ethylene Glycol Clusters Upon Hydration, J. Phys. Chem. A 116 (17) (2012) 4239–4247.
[35] Y. Chen, Y. Ozakib, M.A. Czarnecki, Molecular Structure and Hydrogen Bonding in Pure Liquid Ethylene Glycol and Ethylene Glycol-Water Mixtures Studied Using NIR Spectroscopy, Phys. Chem. Chem. Phys. 15 (2013) 18694–18701.
[36] A. Jindal, S. Vasudevan, Conformation of Ethylene Glycol in the Liquid State: Intra- versus Intermolecular Interactions, J. Phys. Chem. B 121 (2017) 5595–5600.
[37] I. Bako, T. Grosz, G. Palinkas, M.C. Bellissent-Funel, Ethylene Glycol Dimers in the Liquid Phase: A Study by X-Ray and Neutron Diffraction, J. Chem. Phys. 118 (2003) 3215–3221.
[38] K.A. Petterson, R.S. Stein, M.D. Drake, J.D. Roberts, An NMR Investigation of the Importance of Intramolecular Hydrogen Bonding in Determining the Conformational Equilibrium of Ethylene Glycol in Solution, Magn. Reson. Chem. 43 (2005) 225–230.
[39] M.A. Czarnecki, Y. Liu, Y. Ozaki, M. Suzuki, M. Iwahashi, Usefulness of the Second Overtone of the OH Stretching Mode for the Study of the Dissociation of Hydrogen-Bonded Z-9-Octadecen-1-ol in the Pure Liquid State, Appl. Spectrosc. 47 (1993) 2162–2168.
[40] F. Neese, The ORCA Program System, Wiley Interdisc. Rev. Comp. Mol. 2 (1) (2012) 73–78.
[41] F. Neese, Software Update: The ORCA Program System – Version 5.0, Wiley Interdisc, Rev. Comp. Mol. 12 (2022) 1606.
[42] V. Barone, M. Cossi, Quantum Calculation of Molecular Energies and Energy Gradients in Solutionn by a Conductor Solvent Model, J. Phys. Chem. A 102 (1998) 1995–2001.
[43] S. Grimme, S. Ehrlich, L. Goerigk, J. Comput. Chem. 32 (2011) 1456–1465.
[44] S. Grimme, J. Antony, S. Ehrlich, H. Krieg, A Consistent and Accurate ab initio Parametrization of Density Functional Dispersion Correction (DFT-D) for the 94 Elements H-Pu, J. Chem. Phys. 132 (2010), 154104.
[45] K.B. Beć, Y. Futami, M.J. Wójcik, Y. Ozaki, A Spectroscopic and Theoreical Study in the Near-Infrared Region of Low Concentration Aliphatic Alcohols, Phys. Chem. Chem. Phys. 18 (2016) 13666–13682.
[46] D.L. Howard, P. Jørgensen, H.G. Kjaergaard, Weak Intramolecular Interactions in Ethylene Glycol Identified by Vapor Phase OH−Stretching Overtone Spectroscopy, J. Am. Chem. Soc. 127 (48) (2005) 17096–17103.
[47] B. Stuart, Infrared Spectroscopy: Fundamentals and Applications, John Wiley & Sons Ltd, 2004.
[48] L. Geissler, Temperature Dependence of Inhomogeneous Broadening: On the Meaning of Isosbestic Points, J. Am. Soc. 127 (2005) 14930–14935.
[49] F. Khayamim, J. Wetterlind, H. Khademi, A.H.J. Robertson, A.F. Cano, B. o. Stenberg, Using Visible and Near Infrared Spectroscopy to Estimate Carbonates and Gypsum in Soils in Arid and Subhumid Regions of Isfahan, Iran, J. near Infrared Spectrosc. 23 (3) (2015) 155–165.
[50] G.R. Hunt, J.W. Salisbury, Visible and Near Infrared Spectra of Minerals and Rocks: Carbonates, Mod. Geol. 2 (1971) 23.
[51] O.H. Wheeler, Near Infrared Spectra of Organic Compounds, Chem. Rev. 59 (4) (1959) 629–666.
[52] J.W. Ellis, The Near Infrared Spectra of Some Aldehydes, Ketones, Esters and Ethers, J. Am. Chem. Soc. 51 (1929) 1384–1394.
[53] R.A. Nyquist, W.J. Potts, Infrared Absorption Characteristics of Organic Carbonate Derivatives and Related Compounds, Spectrochim. Acta 1061 (1961) 679–697.
[54] Y. Chen, X. Hu, W. Chen, C. Liu, K. Qiao, M. Zu, Y. Lou, T. Mu, High Volatility of Superbase-Derived Eutectic Solvents for CO_2 Capture, Phys. Chem. Chem. Phys. 23 (2021) 2193–2210.